(Received 3 March 2024, Accepted 14 May 2024, Scheduled 26 May 2024)

Wideband Circularly Polarized Exponential Slot Antenna with Rectangular Island for X-Band Satellite Applications

Mostafa Mahmoud Rabie[1, 2, *], Mohamed S. El-Gendy[3], Angie R. Eldamak[2], Fawzy Ibrahim[4], and Hadia El-Henawy[2]

[1] *Electrical and Electronics Engineering Coventry University, Cairo, Egypt*
[2] *Electronics and Communications Engineering Department, Ain Shams University, Cairo, Egypt*
[3] *Electronics Research Institute, Cairo, Egypt*
[4] *Egyptian Academy for Engineering and Advanced Technology, Cairo, Egypt*

ABSTRACT: This paper introduces a compact, circularly polarized exponential slot antenna with a rectangular island. The concept of the proposed antenna is similar to that of fractal antennas as it is based on designing an asymmetric slot shape with an increased electrical length within a small area, thanks to the exponential path. The obtained results are as follows. The reflection-coefficient $|S_{11}|$ of the proposed antenna covers the band from 5.5 GHz to 9 GHz. The proposed antenna is circularly polarized with an axial-ratio (AR) bandwidth that extends from 6.87 GHz to 8.9 GHz. It offers simultaneous dual circular polarizations (RHCP and LHCP). The gain of the proposed antenna varies between 4.2 dBic and 5.4 dBic. The efficiency reaches 94%. The size of the antenna is compact making it suitable for CubeSats with limited surface area. The proposed antenna intended application is X-band Earth-Space satellite communication. The proposed antenna can be employed for both the X-band satellite downlink (from 7.25 GHz to 7.75 GHz) and uplink (from 7.9 GHz to 8.4 GHz) frequency bands. Additionally, the antenna can be utilized in military applications, and RFID tag tracking equipment. A prototype of the proposed antenna has been fabricated and then measured using Vector Network Analyzer (VNA) and inside an anechoic chamber. The measurement results of the proposed antenna are in excellent match with the simulated ones.

1. INTRODUCTION

The utilization of X-band technology is widespread across various applications due to its ability to transmit data at high rates, operate over short distances, and provide large bandwidths. However, designing X-band antennas that meet the specific requirements of these applications remains a challenge [1–5]. There is a growing demand for compact and lightweight antennas that can be easily integrated into modern communication systems. Planar antennas have gained extensive use in advanced satellite and wireless communication devices due to their low cost, low profile, and ease of fabrication [6, 7]. However, planar antennas have limitations such as small bandwidth, low power handling capacity, and low gain [6]. Consequently, achieving wide bandwidth, acceptable gain, and small antenna size presents a challenging objective.

Satellites play an increasingly important role in various fields, including communication, oceanography, agriculture, astronomy, positioning, and surveillance [8, 9]. Satellites are classified based on their size, with the smallest being femto-satellites weighing less than 0.1 kg [10]. The design of satellite antennas differs from antennas used in other applications, as the size, shape, and weight constraints imposed by satellites are critical factors to consider [11]. Modern satellite communication systems require antennas that are very small and have low cost, low profile, and high gain. Planar antennas are particularly desirable for satellite communication systems due to their low profile, lightweight nature, ease of fabrication, robustness, ability to be easily installed on various mounting surfaces, and compatibility with microwave monolith integrated circuits (MMICs) and optoelectronics integrated circuits (OEICs) technologies. Planar antennas also offer adaptability in terms of resonance frequency, polarizations, impedance, and radiation patterns, making them attractive for many applications [6, 7, 12].

Circular polarization is a highly advantageous property that finds widespread applications in various fields. One primary advantage is its ability to overcome the unwanted effects of multipath interference by rejecting signals with an opposite-handedness polarization. This property makes circular polarization highly effective in mitigating interference caused by reflected signals [13]. Additionally, circularly polarized (CP) signals are robust in communication links, as they are not affected by polarization misalignment between transmitting and receiving antennas, unlike linearly polarized radiators. This makes CP signals advantageous in situations where the relative orientation between antennas is variable, such as in satellite communications [14].

Various antenna designs have been investigated for X-band satellite applications. The first antenna [2] is a compact telemetry antenna with dual circular polarizations. It covers a bandwidth from 8.025 GHz to 8.4 GHz, with a 3-dB axial ratio (AR) bandwidth of 370 MHz and a maximum gain of 5 dBi. Although the antenna has a relatively large size with a diameter of

* Corresponding author: Mostafa Mahmoud Rabie (ad8259@coventry.ac.uk).

238 mm ($6.52\lambda_0$) and a height of 185 mm ($5.13\lambda_0$), it achieves a good gain. The second antenna [3] is a superstrate antenna suitable for CubeSat applications. It has a bandwidth from 8 GHz to 9.7 GHz, a 3-dB AR bandwidth of 580 MHz, and a maximum gain of 14 dBi. The antenna size is $62 \times 62 \times 22\,\text{mm}^3$ ($1.77\lambda_0 \times 1.77\lambda_0 \times 0.63\lambda_0$), which is considered large, mainly due to the large antenna thickness. The third antenna [15] is a telemetry circularly polarized antenna designed for CubeSats. It has a bandwidth from 8 GHz to 8.4 GHz, a 3-dB AR bandwidth of 400 MHz, and a maximum gain of 5 dBi. The antenna size is $100 \times 100 \times 15\,\text{mm}^3$ ($2.74\lambda_0 \times 2.74\lambda_0 \times 0.41\lambda_0$), which is relatively large compared to the achieved gain. The fourth antenna [4] is a metasurface (MS)-based antenna for X-band satellite communications. It has a bandwidth from 7 GHz to 8.9 GHz, a 3-dB AR bandwidth of 1.15 GHz, and a maximum gain of 8.6 dBi. The antenna has a diameter of 50 mm ($1.3\lambda_0$) and a height of 5.25 mm ($0.137\lambda_0$). The fifth antenna [1] is a broadband substrate integrated waveguide antenna for X-band synthetic aperture radar (SAR) applications. It has a bandwidth from 9.4 GHz to 10.5 GHz, achieves a maximum gain of 9 dBi, but does not achieve circular polarization. The antenna size is $59 \times 14 \times 0.76\,\text{mm}^3$ ($1.96\lambda_0 \times 0.46\lambda_0 \times 0.025\lambda_0$). The sixth antenna described in [16] is a planar antenna designed for X-band SAR applications on small satellites. It offers a wide bandwidth ranging from 9.01 GHz to 10.2 GHz and achieves a maximum gain of 8 dBi. However, it does not provide circular polarization. The antenna's physical dimensions are $14 \times 14 \times 3.986\,\text{mm}^3$ ($0.45\lambda_0 \times 0.45\lambda_0 \times 0.126\lambda_0$).

This paper focuses on developing and analyzing a circularly polarized exponential slot antenna with a rectangular island, specifically tailored for X-band satellite applications. The proposed antenna design incorporates an exponential slot shape and features an embedded rectangular island to enhance overall performance characteristics. This design aims to achieve increased bandwidth for the reflection coefficient, gain enhancement, and improved axial ratio bandwidth.

The proposed antenna design is required to cover the X-band satellite uplink from 7.25 GHz to 7.75 GHz and downlink from 7.9 GHz to 8.4 GHz for satellite communication application. The proposed antenna is designed to achieve circular polarization all over its operating band with a wide axial ratio (AR) bandwidth.

The use of an exponential slot shape offers several advantages in achieving circular polarization. By introducing asymmetry into the slot shape, the electric field distribution becomes nonuniform, resulting in the generation of orthogonal radiation components with a phase difference of 90 degrees [17]. This phase difference is essential for circular polarization, enabling the antenna to transmit and receive signals with optimal polarization characteristics [17]. The concept presented here draws inspiration from fractal antennas, which have demonstrated the ability to achieve broad bandwidths and circular polarization within compact antenna designs [18–20]. The utilization of an exponential shape slot offers distinct advantages such as an increased effective length compared to straight lines slot. This exponential curve, combined with an asymmetrical structure, contributes to achieving wide bandwidths and circular polarization. By incorporating an exponential shape, antennas can effectively increase their effective length. This longer effective length enhances the antenna's radiation efficiency and enables broader frequency coverage.

The embedded islands inside slot antennas serve to enhance the antenna's bandwidth and circular polarization by widening the AR bandwidth. Additionally, the embedded islands can enhance the antenna's gain and directivity by providing additional resonant structures. Overall, an embedded island contributes to the improved performance and functionality of slot antennas [21–24]. This paper is organized as follows. The design procedure is presented in Section 2. Results and analysis are introduced in Section 3. The proposed antenna design and experimental results are given in Section 4. Final assessment and comparison with recent X-band antenna designs are introduced in Section 5. Conclusion is presented in Section 6.

2. DESIGN PROCEDURE

The proposed antenna is composed of three layers. An exponential slot and rectangular island are on the top layer. The feedline exists in the bottom layer. The substrate layer exists in between as shown in Figure 2. The substrate used is Rogers-RT-Duroid-5880 with dielectric constant ε_r of 2.2, loss tangent of 0.0009, and thickness of 0.508 mm. The overall length L and width W of the proposed antenna are selected to be slightly greater than the height of the exponential slot as shown in Figure 2(a). The design procedure is presented in the following three steps.

2.1. Step 1: Exponential Slot Design

An exponential slot as shown in Figure 1 is designed with a base width, SW equivalent to half the guided wavelength, λ_g which is the conventional slot antenna width [25, 26, 17]. The reason behind selecting an exponential slot shape is to provide asymmetry to the slot shape to achieve circular polarization. The exponential slot is designed so that an exponential decaying curve is placed above the slot base such that the starting point of the curve is at a height of SL_1, and the end point of the curve is at a height SL_2 as shown in Figure 1. The exponential slot design starts by calculating the width of the slot SW, then calculating the lengths of the two sides of the slot, SL_1 and SL_2, as shown in Figure 1. Finally, the exponential coefficient constant, k, can be calculated, which determines the rate of decay of the exponential function, $E(x)$. The exponential slot design equations are listed as follows:

$$SW \cong \frac{\lambda_g}{2} \tag{1}$$

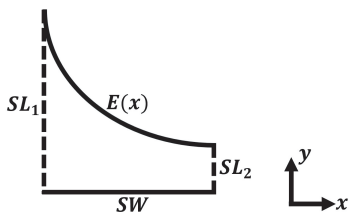

FIGURE 1. Exponential slot realization.

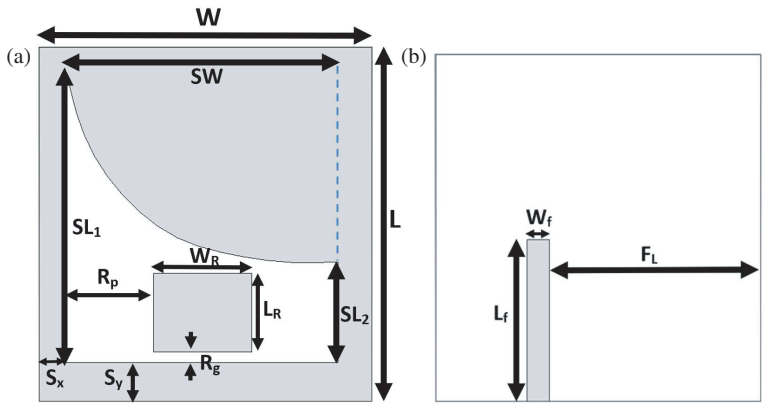

FIGURE 2. Exponential slot antenna with rectangular embedded island: (a) Front view and (b) Back view.

$$SL_2 \cong \frac{\lambda_g}{4} \tag{2}$$

$$SL_1 > \frac{\lambda_g}{4} \tag{3}$$

The value of SL_1 is selected to be greater than the value of SL_2 to make the slot shape asymmetric to achieve circular polarization. By increasing the value of SL_1, the asymmetry of the exponential slot increases. The initial value of SL_1 is selected to be approximately equal to three times the value of SL_2. Parametric analyses are performed on SL_1, and optimum results are introduced in the next section.

$$E\left(x\right) = SL_2 e^{-(x-SW)k} \tag{4}$$

SL_1 can be written as follows by substituting x within the exponential function, $E(x)$.

$$SL_1 = E\left(0\right) = SL_2 e^{SWk} \tag{5}$$

The value of k can be determined as follows after calculating the values of SL_1 and SL_2 using Equations (1) and (2).

$$k = \frac{1}{SW} \ln\left(\frac{SL_1}{SL_2}\right) \tag{6}$$

2.2. Step 2: Feedline Configuration

The second step is microstrip feedline configuration. The slot antenna is fed using a microstrip feedline at the bottom layer as shown in Figure 2(b). The length and width of the feedline are L_f and W_f, respectively. The feedline is initially positioned in the middle of the antenna at a distance of F_L from the left side of the antenna as shown in Figure 2(b). In subsection 3.1, parametric analysis is performed to optimize the feed location, F_L, and optimum feed location results are introduced.

2.3. Step 3: Rectangular Island Integration

The third step is placing a rectangular island centered in the middle of the slot. The function of the embedded island is achieving a large bandwidth along with wideband circular polarization (large 3-dB AR-bandwidth). The incorporation of embedded islands within slot antennas serves multiple purposes, each contributing to the enhancement of the antenna's performance and functionality [21–24]. By introducing embedded islands, the slot antenna's bandwidth is widened, leading to an increased range of frequencies over which it can effectively operate. This expansion is attributed to the interaction between the embedded islands and electromagnetic waves, with the islands acting as additional resonators that alter the current distribution within the antenna structure. This improvement results in the antenna maintaining circular polarization across a broader frequency spectrum, enhancing its polarization purity. In addition, the inclusion of embedded islands significantly contributes to the enlargement of the axial ratio (AR) bandwidth. The altered current flow induced by the islands modifies the radiation characteristics of the antenna, introducing additional resonant modes that effectively widen the AR bandwidth. Consequently, the antenna can maintain a consistent circular polarization response over a wider range of frequencies, making it more versatile and effective in diverse operating conditions. The rectangular island is placed at a distance R_p from the left side of the exponential slot and R_g from the bottom side of the exponential slot as shown in Figure 4(a). The embedded rectangular island has a height of L_R and a width of W_R. For the rectangular island to fit within the exponential, it is important to choose the length L_R and width W_R to be less than SL_2 by a specific percentage. The initial values of L_R and W_R are selected to be equal and smaller than $\lambda_g/4$. Parametric analyses are then performed on the dimensions of the rectangular island, L_R and W_R along with its horizontal position R_p to achieve the widest required reflection coefficient $|S_{11}|$ bandwidth along with the widest required AR bandwidth. The parametric analyses and optimum results are introduced in section 3.

3. RESULTS AND ANALYSIS

The proposed design is then simulated and analyzed using CST. The dimensions of the exponential slot opening are calculated at operating frequency f_r equal to 7.8 GHz ($\lambda_0 = 38.46$ mm), which is the center frequency of the required band that extends

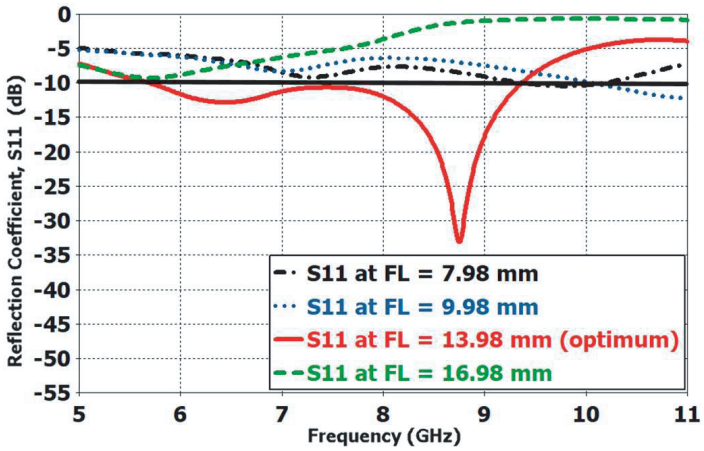

FIGURE 3. Simulated reflection-coefficient $|S_{11}|$ of the exponential slot antenna at different values of F_L.

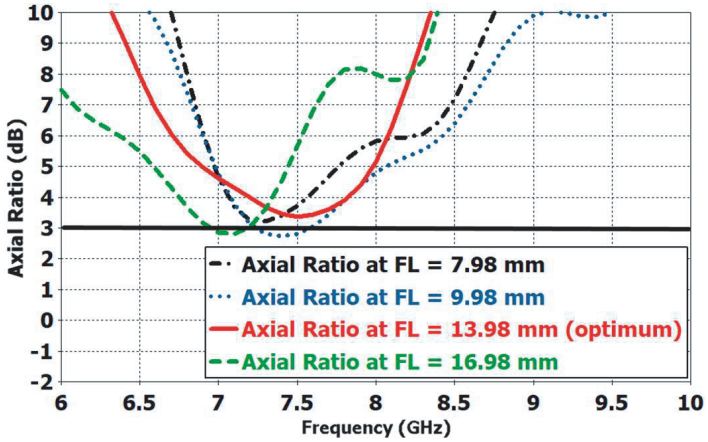

FIGURE 4. Simulated axial-ratio (AR) of the exponential slot antenna at different values of F_L.

from 7.25 GHz to 8.4 GHz using Equations (1)–(6). The optimum feed location is studied in Subsection 3.1. Parametric analyses are then performed on the embedded rectangular island shown in Figure 2, to achieve the widest reflection coefficient $|S_{11}|$ bandwidth along with the widest AR bandwidth. The parametric analyses are performed in three steps. The first step in Subsection 3.2 is performed on the width of the embedded rectangular island, W_R. The second step in in Subsection 3.3 is performed on the height of the embedded rectangular island, L_R. The third step in Subsection 3.4 is performed on the position of the embedded rectangular island, R_p. To begin the parametric analysis, the starting values of L_R and W_R are initially selected to be approximately equal to 6 mm.

3.1. Studying the Optimum Feed Location

First, the exponential slot antenna, shown in Figure 2, is simulated at different values of feed location, F_L, as shown Figure 2(b) to study its effect. The value of F_L that gives a wider bandwidth and wider 3-dB AR bandwidth is then selected. The exponential antenna is simulated at $F_L = 8.35$ mm, 10.9 mm (centered), and 13.4 mm. Figure 3 shows the reflection coefficient $|S_{11}|$ at $F_L = 7.98$ mm, 9.98 mm, 13.98 mm, and 16.98 mm. Figure 4 shows the axial ratio (AR) at $F_L = 7.98$ mm, 9.98 mm, 13.98 mm, and 16.98 mm. The selected value of feed location F_L is 13.98 mm where it provides a properly matched and wide bandwidth of 3.64 GHz extending from 5.73 GHz to 9.37 GHz. It also provides low AR (below 4 dB) at most of the required bandwidth (7.25 GHz–7.75 GHz). The 4 dB AR bandwidth is 600 MHz extending from 7.2 GHz to 7.8 GHz. Improvements to the AR of the exponential slot antenna is required, to make it lower than 3 dB and also to widen the 3 dB AR bandwidth to cover the whole required bandwidth (7.25 GHz–8.4 GHz). The improvements are performed in the upcoming subsections by performing parametric analysis on the width, length, and position of the rectangular island as shown in Figure 2.

3.2. Studying the Effect of Length W_R

A parametric study is performed on W_R while all the other parameters are kept constant. The exponential slot antenna shown in Figure 2 is simulated at different values of W_R. The reflection coefficient $|S_{11}|$ and the AR

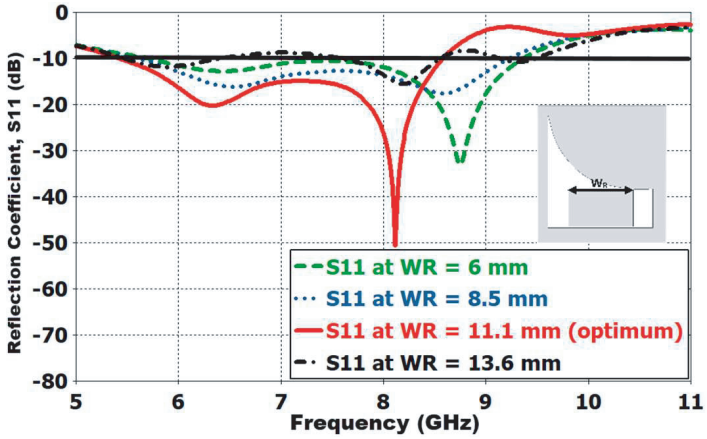

FIGURE 5. Simulated reflection-coefficient $|S_{11}|$ of the exponential slot antenna at different values of W_R.

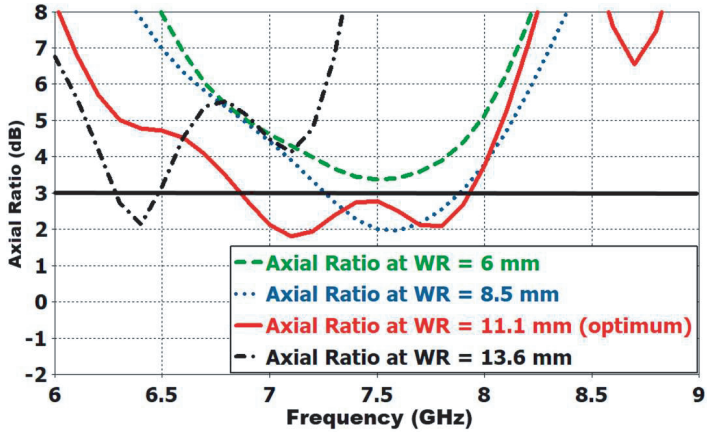

FIGURE 6. Simulated axial-ratio (AR) of the exponential slot antenna at different values of W_R.

curves for different values of W_R are shown in Figure 5 and Figure 6, respectively. It is shown in Figure 5 that the reflection coefficient $|S_{11}|$ bandwidth at $W_R = 6$ mm, 8.5 mm, 11.1 mm, and 13.6 mm is 3.8 GHz (5.5 GHz–9.3 GHz), 3.6 GHz (5.5 GHz–9.1 GHz), 3.1 GHz (5.5 GHz–8.6 GHz), and 900 MHz (7.6 GHz–8.5 GHz), respectively. Figure 6 shows that the AR curve for $W_R = 6$ mm is greater than 3-dB. The 3-dB AR bandwidth at $W_R = 8.5$ mm, 11.1 mm, and 13.6 mm is 600 MHz (7.3 GHz–7.9 GHz), 1.1 GHz (6.8 GHz–7.9 GHz), and 200 MHz (6.2 GHz–6.4 GHz), respectively. $W_R = 11.1$ mm achieves the largest -10-dB reflection coefficient $|S_{11}|$ bandwidth that is common with the largest 3-dB AR bandwidth, reaching 1.1 GHz. Therefore, the selected width of the rectangular island, W_R, is 11.1 mm. In the upcoming subsection, parametric study is performed on L_R to study its effect on the reflection coefficient $|S_{11}|$ bandwidth and the 3-dB AR bandwidth.

3.3. Studying the Effect of Length L_R

After updating the value of W_R, a parametric study is performed on L_R while all the other parameters are kept constant. The exponential slot antenna shown in Figure 2 is simulated at different values of L_R. Any variation in the length of the embedded rectangular island, $L_{R,}$, will change the gap length, R_g, as shown in Figure 2. The reflection coefficient $|S_{11}|$ and the AR curves for different values of L_R are shown in Figure 7 and Figure 8, respectively. It is shown in Figure 7 that the reflection coefficient $|S_{11}|$ bandwidth at $L_R = 4$ mm, 5 mm, and 6 mm is 1.36 GHz (4.77 GHz–6.13 GHz), 1.6 GHz (4.8 GHz–10.85 GHz), and 3.17 GHz (5.4 GHz–8.57 GHz), respectively. Figure 8 shows that the 3-dB AR bandwidth at $L_R = 4$ mm, 5 mm, and 6 mm is 1.25 GHz (6.32 GHz–7.57 GHz), 1.18 GHz (6.32 GHz–7.5 GHz), and 1.1 GHz (6.8 GHz–7.9 GHz), respectively. $L_R = 6$ mm achieves the largest -10-dB reflection coefficient $|S_{11}|$ bandwidth which is common with the largest 3-dB AR bandwidth, reaching 1.1 GHz. Therefore, the selected length of the rectangular island, L_R, is 6 mm. In the upcoming subsection, parametric study is performed on R_p to study its effect on the reflection coefficient $|S_{11}|$ bandwidth and the 3-dB AR bandwidth.

3.4. Studying the Effect of Length R_p

After attuning the length, L_R, and the width, W_R, of the rectangular island to achieve the largest common -10-dB reflection coefficient $|S_{11}|$ and 3-dB AR bandwidth, a parametric study is performed on the rectangular island position

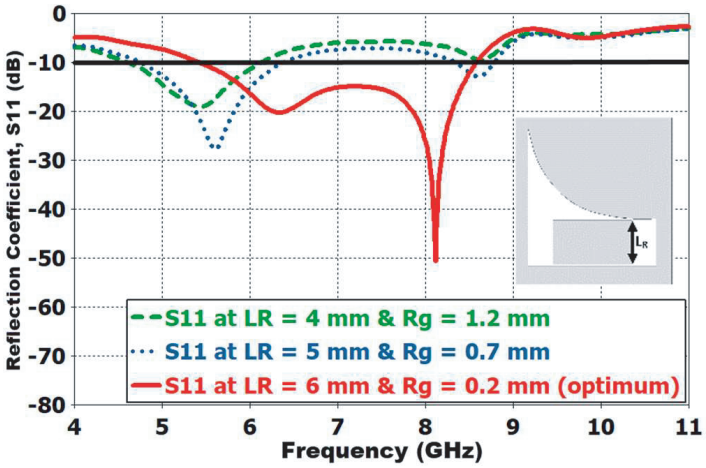

FIGURE 7. Simulated reflection-coefficient $||S_{11}|$ of the exponential slot antenna at different values of L_R.

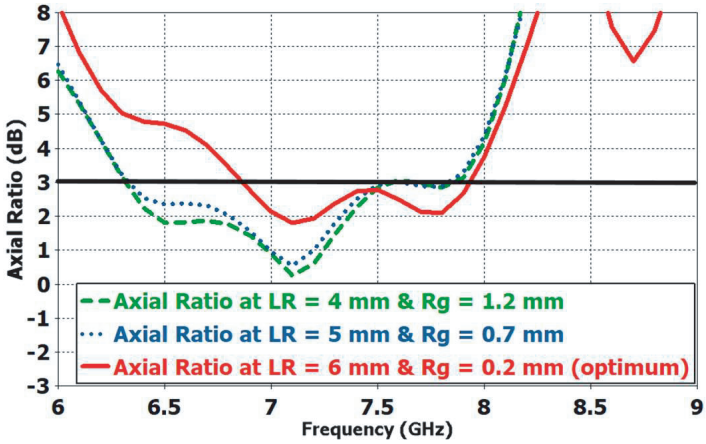

FIGURE 8. Simulated axial-ratio (AR) of the exponential slot antenna at different values of L_R.

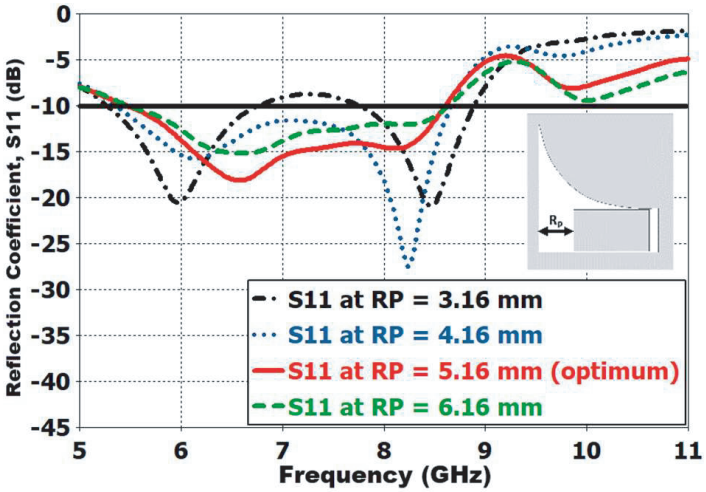

FIGURE 9. Simulated reflection-coefficient $|S_{11}|$ of the exponential slot antenna at different values of R_p.

R_p, while all the other parameters are kept constant. The exponential slot antenna shown in Figure 2 is simulated at different values of R_p. The reflection coefficient $|S_{11}|$ and the axial-ratio (AR) curves for different values of R_p are shown in Figure 9 and Figure 10, respectively. It is shown in Figure 9 that the reflection coefficient $|S_{11}|$ bandwidth at R_p = 3.16 mm, 4.16 mm, 5.16 mm, and 6.16 mm is 1 GHz (7.9 GHz–8.9 GHz), 3.3 GHz (5.3 GHz–8.6 GHz), 3.21 GHz

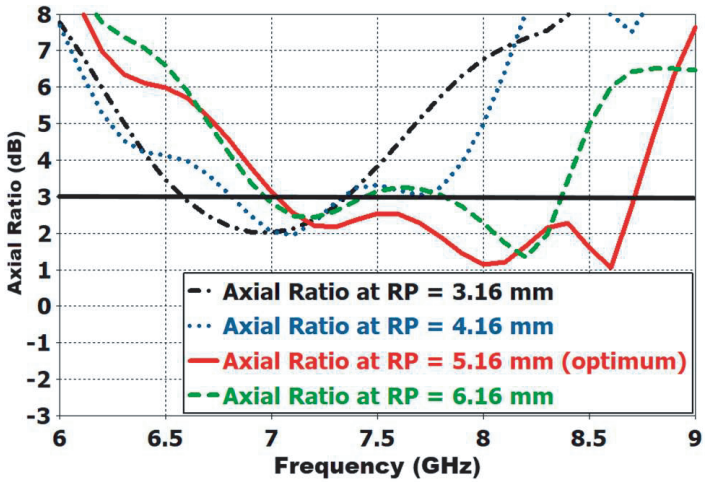

FIGURE 10. Simulated axial-ratio (AR) of the exponential slot antenna at different values of R_p.

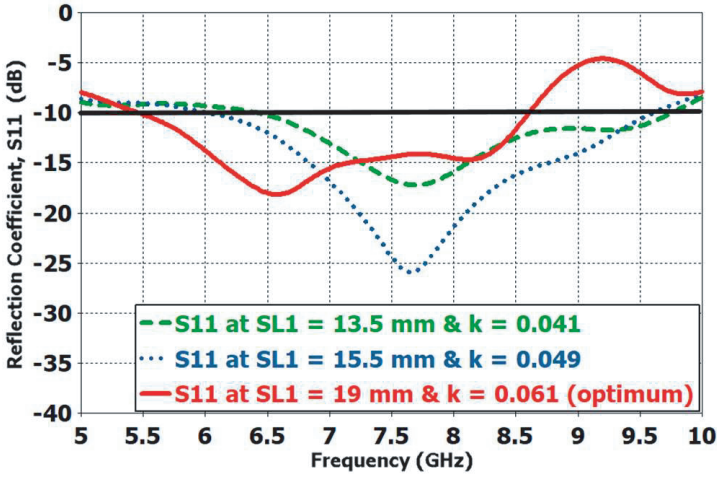

FIGURE 11. Simulated reflection-coefficient $|S_{11}|$ of the exponential slot antenna at different values of SL_1.

(5.4 GHz–8.61 GHz), and 3.2 GHz (5.4 GHz–8.6 GHz), respectively. Figure 10 shows that the 3-dB AR bandwidth at $R_p = 3.16$ mm, 4.16 mm, 5.16 mm, and 6.16 mm is 800 MHz (6.6 GHz–7.4 GHz), 600 MHz (6.8 GHz–7.4 GHz), 1.71 GHz (7 GHz–8.71 GHz), and 1.5 GHz (6.9 GHz–8.4 GHz), respectively. $R_p = 5.16$ mm achieves the largest -10-dB reflection coefficient $|S_{11}|$ bandwidth that is common with the largest 3-dB AR bandwidth, reaching 1.61 GHz with an improvement of 31.67% compared to the results in the previous subsection. Therefore, the selected position of the rectangular island, R_p, is 5.16 mm. In the upcoming subsection parametric study is performed on SL_1 to study its effect on the reflection coefficient $|S_{11}|$ bandwidth and the 3-dB AR bandwidth.

3.5. Studying the Effect of Length SL_1

After selecting the length L_R, the width W_R, and the rectangular island position R_p of the rectangular island to achieve the largest common -10-dB reflection coefficient $|S_{11}|$ and 3-dB AR bandwidth, a parametric study is performed on SL_1, while all the other parameters are kept constant. The exponential slot antenna shown in Figure 2 is simulated at different values of SL_1. Any variation in the value of SL_1 will change the exponential coefficient constant, k, as stated in Equation (6). The reflection coefficient $|S_{11}|$ and the AR curves for different values of SL_1 are shown in Figure 11 and Figure 12, respectively. It is shown in Figure 11 that the reflection coefficient $|S_{11}|$ bandwidth at $SL_1 = 13.5$ mm, 15.5 mm, and 19 mm is 3.3 GHz (6.4 GHz–9.7 GHz), 3.6 GHz (6 GHz–9.6 GHz), and 3.21 GHz (5.4 GHz–8.61 GHz), respectively. Figure 12 shows that the 3-dB AR bandwidth at $SL_1 = 13.5$ mm, 15.5 mm, and 19 mm is 840 MHz (8.31 GHz–9.15 GHz), 710 MHz (8.27 GHz–8.98 GHz), and 1.71 GHz (7 GHz–8.71 GHz), respectively. $SL_1 = 19$ mm achieves the largest -10-dB reflection coefficient $|S_{11}|$ bandwidth which is common with the largest 3-dB AR bandwidth, reaching 1.61 GHz. Therefore, the selected value of SL_1 is 19 mm. The optimized dimensions of the exponential slot antenna are given in Table 1.

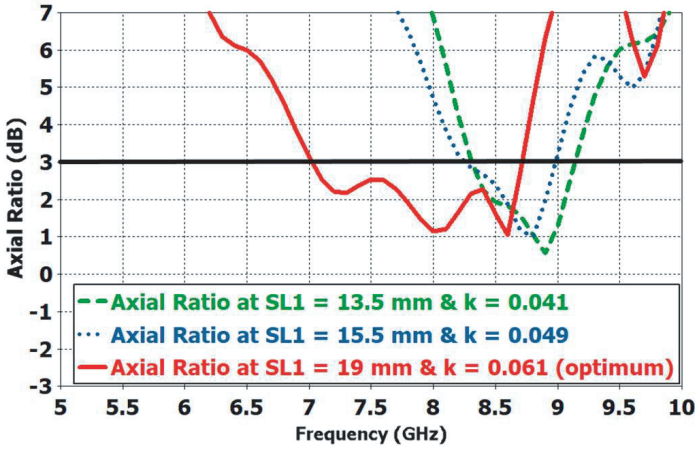

FIGURE 12. Simulated axial-ratio (AR) of the exponential slot antenna at different values of SL_1.

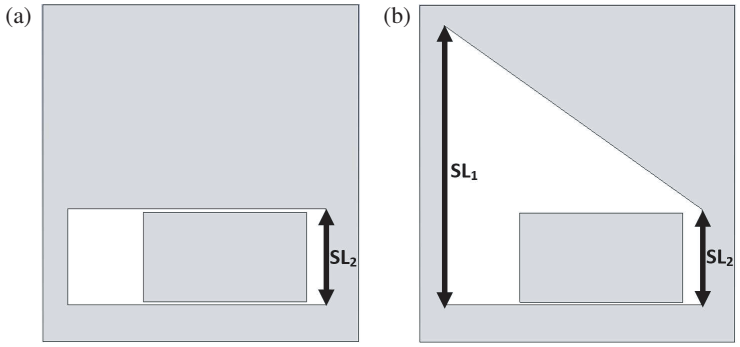

FIGURE 13. Optimized exponential slot antenna variations: (a) Rectangular slot and (b) Asymmetric slot.

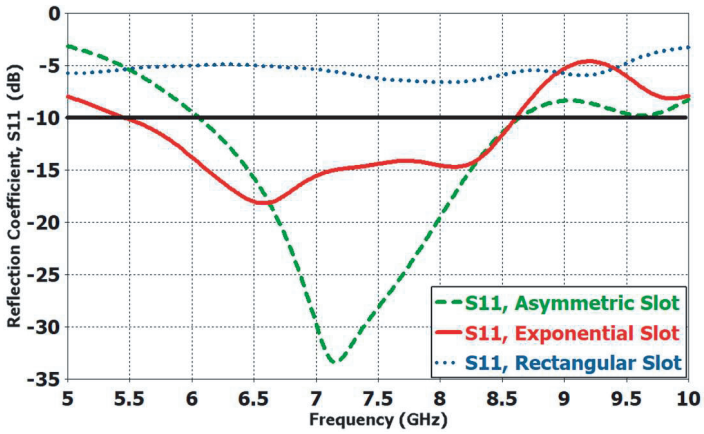

FIGURE 14. Simulated reflection-coefficient $|S_{11}|$ of the exponential slot antenna vs rectangular slot antenna vs asymmetric slot antenna.

3.6. Comparison with Rectangular Slot and Asymmetric Slot Variations

This subsection presents a comparison between the optimized exponential slot antenna and its rectangular slot and asymmetric slot variations as shown in Figure 13. The feed location, embedded rectangular island dimensions, and position are kept constant. This comparison demonstrates the impact of employing the exponential slot, which leads to a broader bandwidth and enables circular polarization with a wide 3-dB AR bandwidth as shown in Figure 14 and Figure 15.

3.7. Design Formulation

This subsection encompasses the design formulation for achieving a targeted circularly polarized frequency band. It specifically considers the guided wavelength, λ_g, that corresponds to the center frequency, f_r, of the desired band.

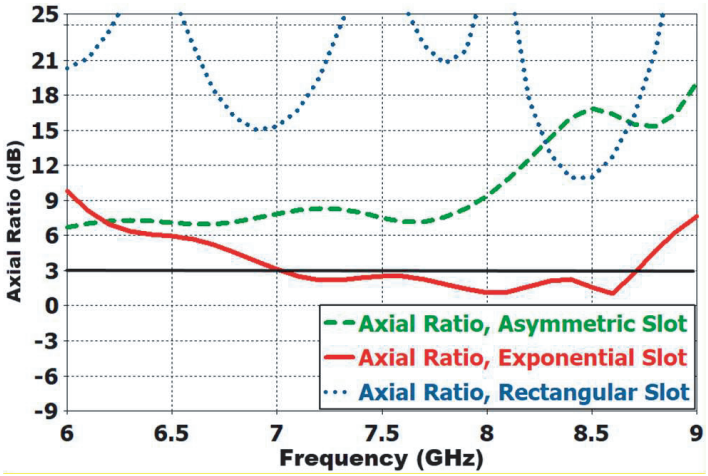

FIGURE 15. Simulated axial-ratio (AR) of the exponential slot antenna vs rectangular slot antenna vs asymmetric slot antenna.

TABLE 1. Optimized dimensions of exponential slot antenna with embedded rectangular island.

Parameter	Value (mm)
SW	17.6
SL_2	6.5
SL_1	19
k	0.061
L_R	6
W_R	11.1
R_g	0.2
R_p	5.16
S_x	1.67
S_y	2.52
L_f	10.67
W_f	1.48
F_L	13.98
L	22.9
W	21.5

By utilizing this formulation, it becomes possible to design antennas that can be effectively employed in a wide range of wireless applications. The design equations are as follows:

$$SW \cong \frac{\lambda_g}{2} \tag{7}$$

$$SL_1 \cong \frac{3\lambda_g}{4} \tag{8}$$

$$SL_2 \cong \frac{\lambda_g}{4} \tag{9}$$

$$E(x) = SL_2 e^{-0.061(x-SW)} \qquad 0 \le x \le SW \tag{10}$$

4. PROPOSED DESIGN AND EXPERIMENTAL RESULTS

This section provides a detailed description of the final design of the proposed exponential slot antenna with an embedded rectangular island. The proposed antenna was fabricated using

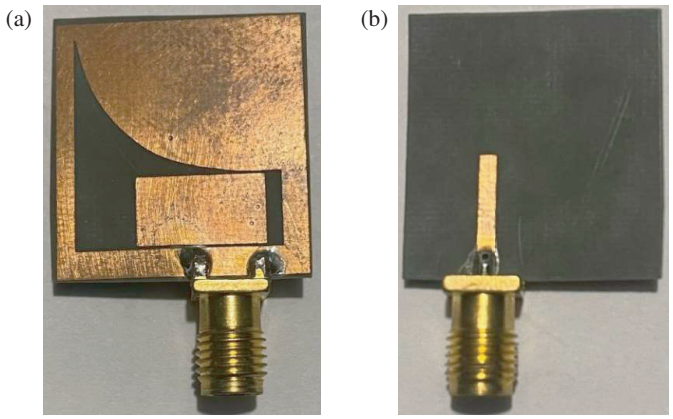

FIGURE 16. Fabricated exponential slot antenna: (a) Front view, (b) Back view.

an RT/Duroid 5880 substrate with dielectric constant $\varepsilon_r = 2.2$, low loss tangent $\tan(\delta) = 0.0009$, and height $h = 0.508$ mm as shown in Figure 16. The antenna's simulated radiation patterns and antenna parameters are presented, as well as the measurements taken from a fabricated prototype of the antenna. The final dimensions of the antenna are given in Table 1. The reflection coefficient $|S_{11}|$ of the antenna was measured using ROHDE & SCHARZ 20 Vector Network Analyzer (VNA) with measurement range up to 20 GHz. The radiation pattern and other antenna parameters were then measured in an anechoic chamber as shown in Figure 17. Simulated and measured radiation patterns and antenna parameters of the exponential slot antenna with an embedded rectangular island were analyzed and compared. To justify the circular polarization property mechanism, the simulated surface currents at 7.5 GHz and 8.15 GHz are shown in Figure 18 and Figure 19, respectively. The surface current distribution of an antenna is an important parameter that determines its radiation characteristics. Figures 18(a), (b), (c), and (d) and Figures 19 (a), (b), (c), and (d) are provided to describe the surface current distribution at phase angles of 0, 90, 180, and 270 degrees, respectively. The maximum surface currents at 7.5 GHz and 8.15 GHz are 182 A/m and 213 A/m, re-

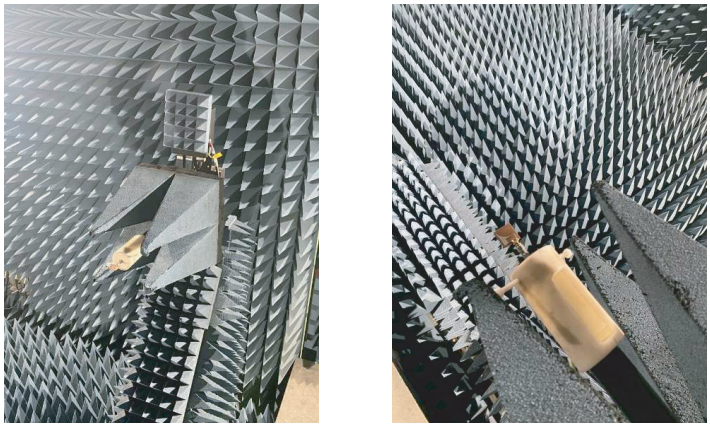

FIGURE 17. Fabricated exponential antenna measurement in the anechoic chamber.

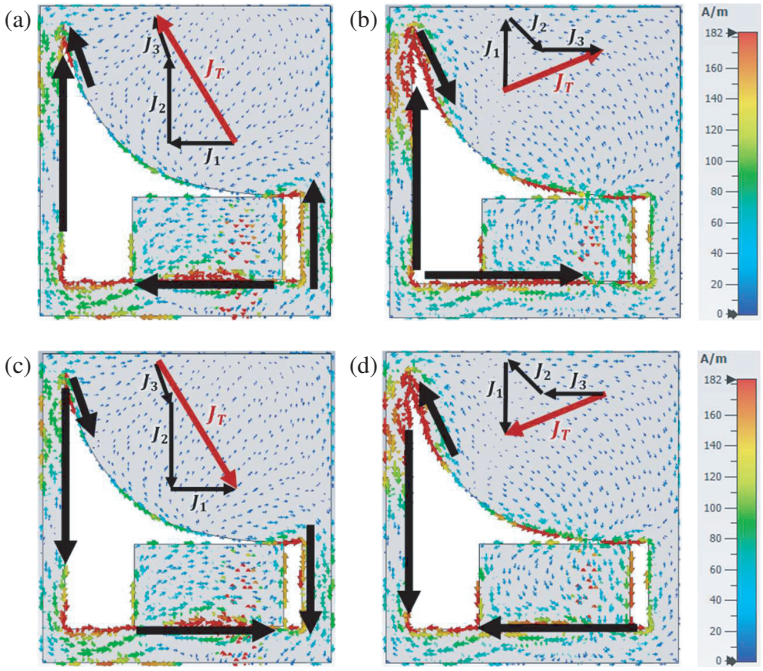

FIGURE 18. Simulated surface current distribution at 7.5 GHz of the exponential slot antenna at phase: (a) 0°, (b) 90°, (c) 180°, (d) 270°.

spectively. The total surface current, J_T, represents the vector summation of all the significant surface current distributions at each phase. It is observed that the total surface currents, J_T, at 0 and 90 degrees are equal in magnitude and opposite in direction to that at 180 and 270 degrees. It can be observed that the total surface current, J_T direction rotates clockwise when comparing each phase to the previous one, and accordingly a left-hand circularly polarized (LHCP) radiation is generated in the positive z direction (antenna front side). The proposed antenna can excite LHCP and RHCP waves [27, 28]. The proposed antenna is a bidirectional simultaneous dual circularly polarized antenna, as it is able to generate a left-hand circular polarization (LHCP) in the positive z direction (antenna front side), whereas a right-hand circular polarization (RHCP) is generated in the negative z direction (antenna back side) at the same time [27–29]. The simulated and measured LHCP and RHCP radiation patterns at 7.5 GHz and 8.15 GHz are shown in Figure 20 and Figure 21, respectively. The simulated and measured axial ratios (ARs) vs theta of the exponential slot antenna at (phi $=$ 0) and (phi $=$ 90) are shown in Figure 22.

The simulated and measured radiation patterns and antenna parameters of the exponential slot antenna with an embedded rectangular island antenna are analyzed and compared. The radiation patterns E-plane (phi $=$ 0) and H-plane (phi $=$ 90) at frequencies of 7.5 GHz and 8.15 GHz for the simulated and fabricated antennas are shown in Figures 23(a), (b), (c), and (d), respectively. The simulated and measured reflection coefficients $|S_{11}|$ are shown in Figure 24 with -10 dB reflection coefficient $|S_{11}|$ bandwidths of 3.21 GHz extending from 5.4 GHz to 8.61 GHz and 3.44 GHz extending from 5.56 GHz to 9 GHz,

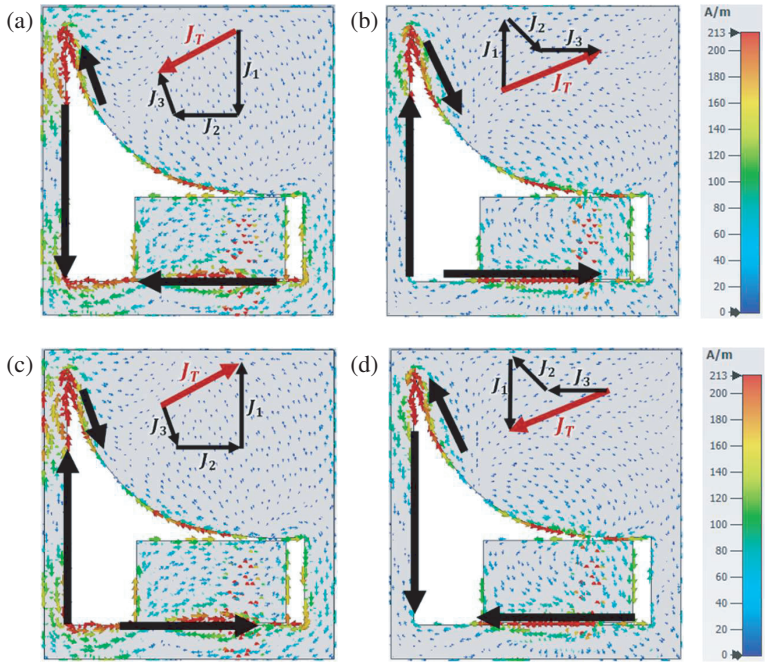

FIGURE 19. Simulated surface current distribution at 8.15 GHz of the exponential slot antenna at phase: (a) 0°, (b) 90°, (c) 180°, (d) 270°.

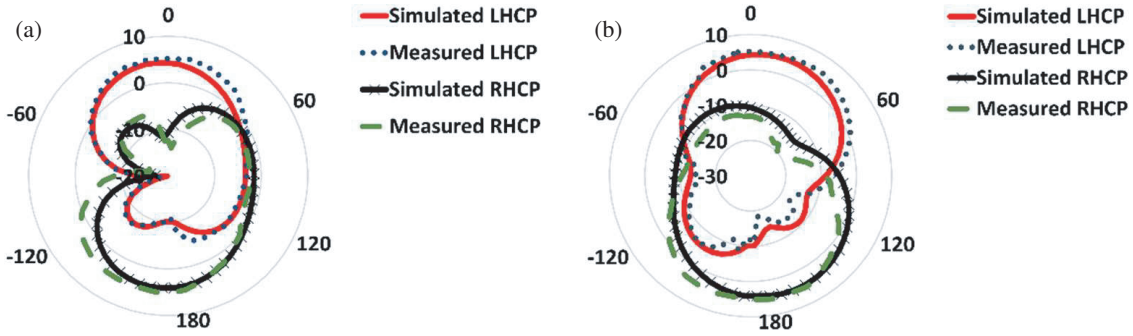

FIGURE 20. Simulated and measured LHCP and RHCP, radiation patterns at 7.5 GHz: (a) E-plane (phi = 0°), (b) H-plane (phi = 90°).

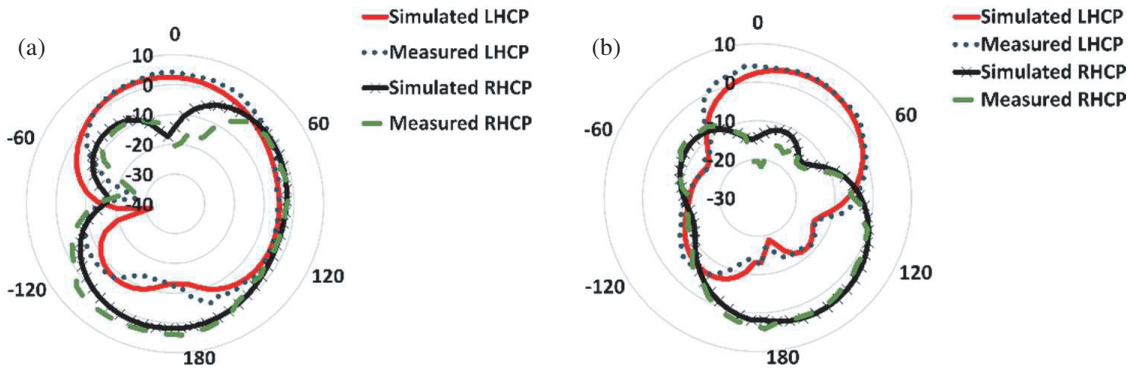

FIGURE 21. Simulated and measured LHCP and RHCP, radiation patterns at 8.15 GHz: (a) E-plane (phi = 0°), (b) H-plane (phi = 90°).

respectively. The simulated and measured axial ratios (ARs) are shown in Figure 25 indicating that the antenna is circularly polarized in the required band. The simulated and measured AR 3-dB bandwidths are 1.71 GHz extending from 7 GHz to 8.71 GHz and 2.03 GHz extending from 6.87 GHz to 8.9 GHz, respectively. The simulated and measured gains are shown in Figure 26 with maximum gains of 4.48 dBic and 5.07 dBic, respectively. The simulated and measured total efficiencies are

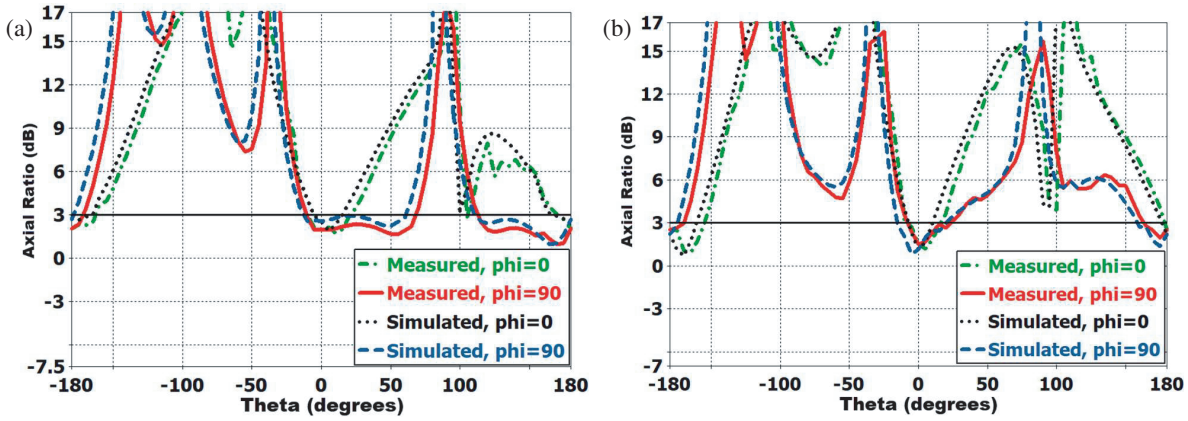

FIGURE 22. Simulated and measured axial-ratio (AR) vs theta of the exponential slot antenna at: (a) 7.5 GHz and (b) 8.15 GHz.

TABLE 2. Comparison with most recent designs of X-band antennas.

Reference	Bandwidth (Hz)	Axial-ratio 3-dB Bandwidth (Hz)	Dual CP	Maximum Gain (dBi)	Antenna Size (mm^3)
[1]	9.4–10.5 GHz (1.1 GHz)	Not Circularly Polarized	No	9 dBi	(Length × Width × Height): 59 mm × 14 mm × 0.76 mm ($1.96\lambda_0 \times 0.46\lambda_0 \times 0.025\lambda_0$)
[2]	8.025–8.4 GHz (370 MHz)	8.025–8.4 GHz (370 MHz)	Yes	5 dBic	Diameter: 238 mm ($6.52\lambda_0$) Height: 185 mm ($5.13\lambda_0$)
[3]	8–9.7 GHz (1.7 GHz)	8.3–8.88 GHz (580 MHz)	No	14 dBic	(Length × Width × Height): 62 mm × 62 mm × 22 mm ($1.77\lambda_0 \times 1.77\lambda_0 \times 0.63\lambda_0$)
[4]	6.8–8.9 GHz (2.1 GHz)	7–8.15 GHz (1.15 GHz)	No	8.6 dBic	Diameter: 50 mm ($1.3\lambda_0$) Height: 5.25 mm ($0.137\lambda_0$)
[15]	8–8.4 GHz (400 MHz)	8–8.4 GHz (400 MHz)	No	5 dBic	(Length × Width × Height): 100 mm × 100 mm × 15 mm ($2.74\lambda_0 \times 2.74\lambda_0 \times 0.41\lambda_0$)
[16]	9.01–10.2 GHz (1.19 GHz)	Not Circularly Polarized	No	8 dBi	(Length × Width × Height): 14 mm × 14 mm × 3.986 mm ($0.45\lambda_0 \times 0.45\lambda_0 \times 0.126\lambda_0$)
[18]	2.57–4.16 GHz (1.59 GHz)	3.09–4.13 GHz (1.04 GHz)	Yes	3.56 dBic	(Length × Width × Height): 40 mm × 40 mm × 1.52 mm ($0.44\lambda_0 \times 0.44\lambda_0 \times 0.17\lambda_0$)
[27]	2–3.5 GHz (1.5 GHz)	2.42–3.3 GHz (880 MHz)	Yes	2.8 dBic	(Length × Width × Height): 55 mm × 49 mm × 1.5 mm ($0.504\lambda_0 \times 0.449\lambda_0 \times 0.013\lambda_0$)
[28]	4.5–7 GHz (2.5 GHz)	4.2–6.5 GHz (2.3 GHz)	Yes	2 dBic	(Length × Width × Height): 20 mm × 20 mm × 1 mm ($0.38\lambda_0 \times 0.38\lambda_0 \times 0.19\lambda_0$)
This work	5.56–9 GHz (3.44 GHz)	6.87–8.9 GHz (2.03 GHz)	Yes	5.4 dBic	(Length × Width × Height): 22.9 mm × 21.5 mm × 0.508 mm ($0.59\lambda_0 \times 0.55\lambda_0 \times 0.013\lambda_0$)

shown in Figure 27 with maximum efficiencies of 94% and 96%, respectively. This indicates that the proposed antenna design is well optimized and capable of achieving excellent performance in terms of efficient use of the available power. The results demonstrate that the measured parameters and radiation patterns of the fabricated antenna match the simulation results, achieving the desired design requirements.

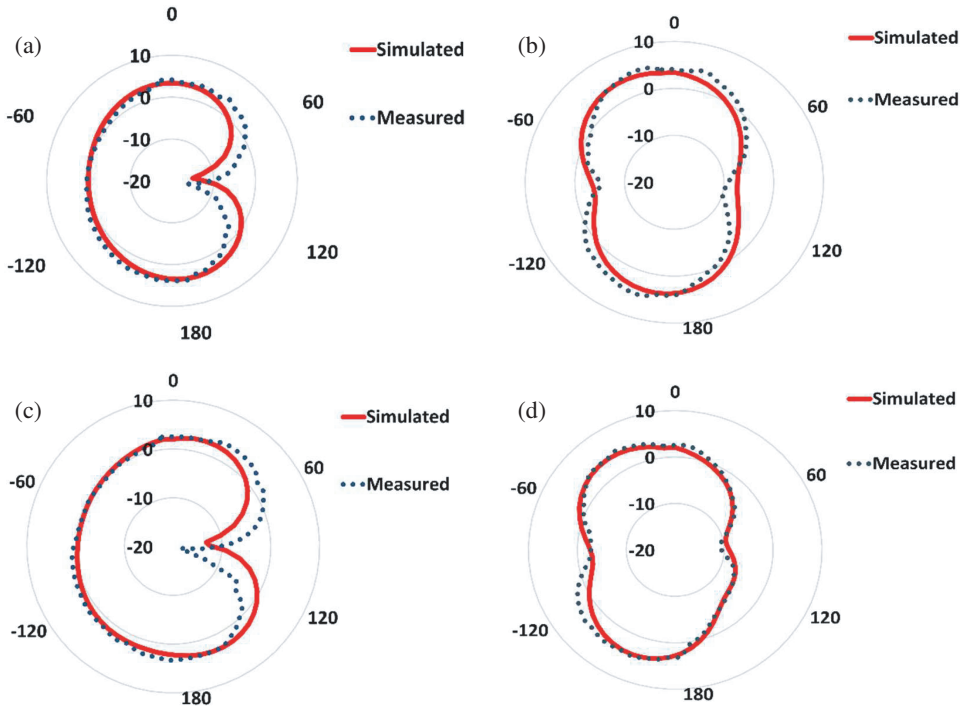

FIGURE 23. Measured vs simulated radiation pattern polar plot (theta vs dBi): (a) E-plane (phi $=0$) at 7.5 GHz, (b) H-plane (phi $=90$) at 7.5 GHz, (c) E-plane (phi $=0$) at 8.15 GHz, (d) H-plane (phi $=90$) at 8.15 GHz.

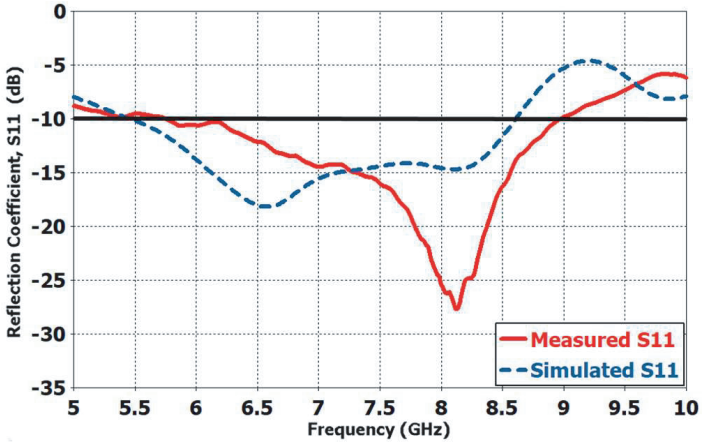

FIGURE 24. Measured vs simulated reflection-coefficient $|S_{11}|$ of the exponential slot antenna.

5. FINAL ASSESSMENT AND COMPARISON WITH RECENT X-BAND ANTENNA DESIGNS

This section presents a comprehensive comparison of the proposed, exponential slot antenna with rectangular island, with several recent X-band antenna designs and antennas with similar configurations as given in Table 2. The proposed design shows remarkable performance in terms of bandwidth, small size, and circular polarization in the required band. The table provides a detailed comparison of different antenna designs in terms of bandwidth, AR 3-dB bandwidth, maximum gain, and antenna size. It is evident that the proposed design outperforms other designs in terms of bandwidth, with a bandwidth of 3.44 GHz extending from 5.56 GHz to 9 GHz, which is exceptionally wide compared to the other designs. Moreover, the proposed design achieves a wideband circular polarization with a 3-dB AR of 2.03 GHz extending from 6.87 GHz to 8.9 GHz. The proposed design also demonstrates a small size with dimensions of 22.9 mm $\times$ 21.5 mm $\times$ 0.508 mm ($0.59\lambda \times 0.55\lambda \times 0.013\lambda$), which is significantly smaller than most of the other designs while still achieving a maximum gain of 5.4 dBic. The antenna design being proposed is suitable for both the downlink (7.25 GHz–7.75 GHz) and uplink (7.9 GHz–8.4 GHz) frequency bands in the X-band satellite communication. The results of our study demonstrate that our proposed X-band antenna design offers superior performance compared to existing designs and has the potential to advance the field of X-band applications significantly.

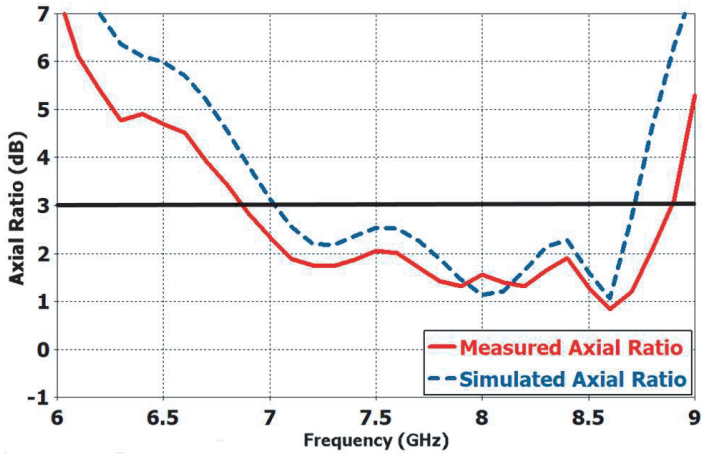

FIGURE 25. Measured vs simulated axial-ratio (AR) of the exponential slot antenna.

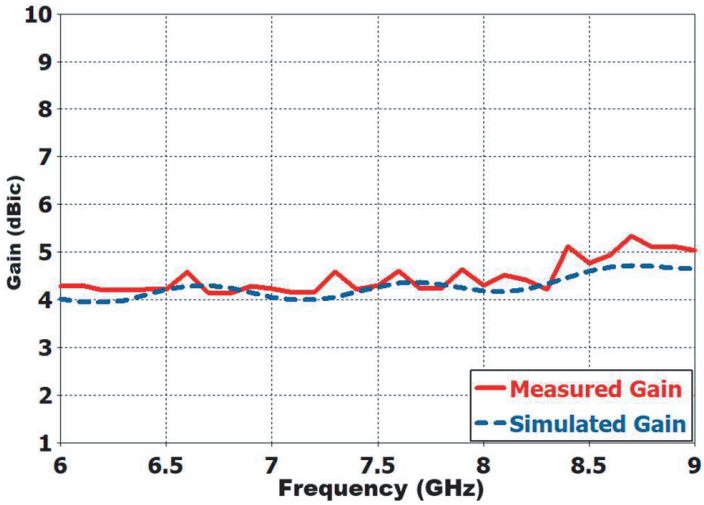

FIGURE 26. Measured vs simulated gain of the exponential slot antenna.

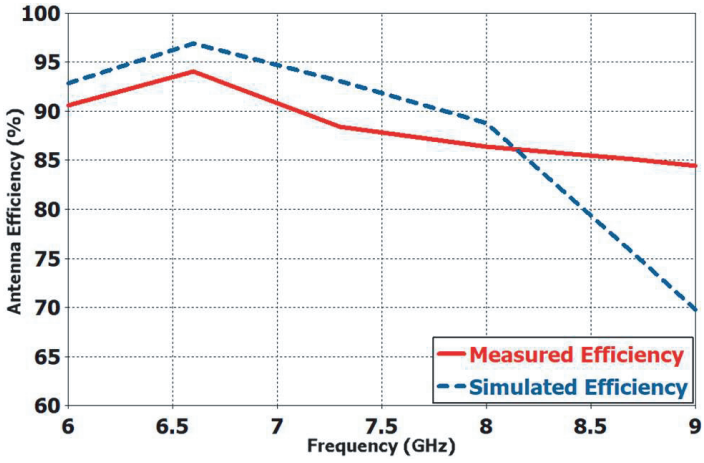

FIGURE 27. Measured vs simulated antenna efficiency of the exponential slot antenna.

6. CONCLUSION

This paper presents the design, simulation, fabrication, and testing of an exponential slot antenna with embedded rectangular island. It introduces and demonstrates the design of an exponential slot antenna that uses a rectangular embedded island for enhancing the bandwidth and axial ratio (AR) of the exponential slot. The designed antenna achieved a wide bandwidth of 3.44 GHz, covering the X-band range from 5.56 GHz to 9 GHz. It also exhibited circular polarization with simultaneous dual circular polarizations (RHCP and LHCP). The AR 3-dB bandwidth was measured to be 2.03 GHz ranging from 6.87 GHz to 8.9 GHz. The antenna design is particularly suitable for both the X-band satellite downlink (from 7.25 GHz to 7.75 GHz) and uplink (from 7.9 GHz to 8.4 GHz) frequency bands. The proposed antenna realized a maximum gain of 5.4 dBi, with the overall size of $22.9 \times 21.5 \times 0.508\,\text{mm}^3$. The compactness and efficiency of the design are noteworthy, with a total antenna efficiency of 96%. These results show that the proposed antenna design is well optimized and capable of delivering outstanding performance. Equivalent circuit model of the exponential slot antenna with embedded rectangular island is introduced. The reliability of the design approach was verified through measurements on a fabricated prototype, further validating its effectiveness.

REFERENCES

[1] El khamlichi, D., N. A. Touhami, T. Elhamadi, and M. A. Ennasar, "High-gain and broadband siw cavity-backed slots antenna for X-band applications," *International Journal of Microwave and Wireless Technologies*, Vol. 13, No. 10, 1078–1085, 2021.

[2] Arnaud, E., J. Dugenet, K. Elis, A. Girardot, D. Guihard, C. Menudier, T. Monediere, F. Roziere, and M. Thevenot, "Compact isoflux X-band payload telemetry antenna with simultaneous dual circular polarization for LEO satellite applications," *IEEE Antennas and Wireless Propagation Letters*, Vol. 19, No. 10, 1679–1683, 2020.

[3] Leszkowska, L., M. Rzymowski, K. Nyka, and L. Kulas, "High-gain compact circularly polarized X-band superstrate antenna for CubeSat applications," *IEEE Antennas and Wireless Propagation Letters*, Vol. 20, No. 11, 2090–2094, 2021.

[4] Genovesi, S. and F. A. Dicandia, "Characteristic modes analysis of a near-field polarization-conversion metasurface for the design of a wideband circularly polarized X-band antenna," *IEEE Access*, Vol. 10, 88 932–88 940, 2022.

[5] Yadav, M. V., S. Baudha, and S. C. Singam, "Multiple slot planar antenna for X-band satellite mobile communication," in *2020 IEEE 7th Uttar Pradesh Section International Conference on Electrical, Electronics and Computer Engineering (UPCON)*, 1–4, 2020.

[6] Adhitya, G., V. Abishek, R. M. Sundaram, and D. P. Jothilakshmi, "Design of microstrip antenna for X band satellite communications," *International Journal of Research and Analytical Reviews*, Vol. 6, No. 2, 342–344, May 2019.

[7] Imbriale, W. A., S. Gao, and L. Boccia, *Space Antenna Handbook*, John Wiley & Sons, 2012.

[8] Van Zyl, J., "Application of satellite remote sensing data to the monitoring of global resources," in *2012 IEEE Technology Time Machine Symposium (TTM)*, 1–1, Dresden, Germany, 2013.

[9] May, S., https://www.nasa.gov/audience/forstudents/5-8/features/nasa-knows/what-is-a-satellite-58.html, 2017.

[10] Xue, Y., Y. Li, J. Guang, X. Zhang, and J. Guo, "Small satellite remote sensing and applications — History, current and future," *International Journal of Remote Sensing*, Vol. 29, No. 15, 4339–4372, 2008.

[11] Hwang, Y., "Satellite antennas," *Proceedings of the IEEE*, Vol. 80, No. 1, 183–193, 1992.

[12] Khac, K. N., N. D. Phong, L. H. Manh, T. A. L. Trong, H. L. Huu, B. T. T. Hien, and D. N. Chien, "A design of circularly polarized array antenna for X-band cubesat satellite communication," in *2018 International Conference on Advanced Technologies for Communications (ATC)*, 53–56, Ho Chi Minh City, Vietnam, 2018.

[13] Dicandia, F. A., S. Genovesi, and A. Monorchio, "Analysis of the performance enhancement of MIMO systems employing circular polarization," *IEEE Transactions on Antennas and Propagation*, Vol. 65, No. 9, 4824–4835, 2017.

[14] Lin, W. and H. Wong, "Wideband circular-polarization reconfigurable antenna with L-shaped feeding probes," *IEEE Antennas and Wireless Propagation Letters*, Vol. 16, 2114–2117, 2017.

[15] Fouany, J., M. Thevenot, E. Arnaud, F. Torres, C. Menudier, T. Monediere, and K. Elis, "New concept of telemetry X-band circularly polarized antenna payload for CubeSat," *IEEE Antennas and Wireless Propagation Letters*, Vol. 16, 2987–2991, 2017.

[16] Anim, K., P. Danuor, S.-O. Park, and Y.-B. Jung, "High-efficiency broadband planar array antenna with suspended microstrip slab for X-band SAR onboard small satellites," *Sensors*, Vol. 22, No. 1, 252, 2022.

[17] Balanis, C. A., *Antenna Theory: Analysis and Design*, John Wiley & Sons, 2016.

[18] Altaf, A., Y. Yang, K.-Y. Lee, and K. C. Hwang, "Wideband circularly polarized spidron fractal slot antenna with an embedded patch," *International Journal of Antennas and Propagation*, Vol. 2017, 2017.

[19] Kwon, O. H., W. B. Park, S. Lee, J. M. Lee, Y. M. Park, and K. C. Hwang, "3D-printed super-wideband spidron fractal cube antenna with laminated copper," *Applied Sciences*, Vol. 7, No. 10, 979, 2017.

[20] Karmakar, A., "Fractal antennas and arrays: A review and recent developments," *International Journal of Microwave and Wireless Technologies*, Vol. 13, No. 2, 173–197, 2021.

[21] Anantrasirichai, N., S. Chanoodhorm, J. Nakasuwan, P. Rakluea, and T. Wakabayashi, "Designing rectangular slot loop antenna for WLAN application," in *TENCON 2005 — 2005 IEEE Region 10 Conference*, 1–5, Melbourne, VIC, Australia, 2005.

[22] Trinh-Van, S., Y. Yang, K.-Y. Lee, Y. S. Kim, and K. C. Hwang, "Bandwidth-enhanced circularly polarized crescent-shaped slot antenna via circular-patch loading," *Applied Sciences*, Vol. 9, No. 6, 1117, 2019.

[23] Kumar, B., B. K. Shukla, A. Somkuwar, and O. P. Meena, "Analysis of hexagonal wide slot antenna with parasitic element for wireless application," *Progress In Electromagnetics Research C*, Vol. 94, 145–159, 2019.

[24] Abed, A. T., M. S. J. Singh, and A. M. Jawad, "Investigation of circular polarization technique in Q-slot antenna," *International Journal of Microwave and Wireless Technologies*, Vol. 12, No. 2, 176–182, 2020.

[25] Sun, X.-b., M.-y. Cao, J.-j. Hao, and Y.-j. Guo, "A rectangular slot antenna with improved bandwidth," *AEU — International Journal of Electronics and Communications*, Vol. 66, No. 6, 465–466, 2012.

[26] Moitra, S., A. K. Mukhopadhyay, and A. K. Bhattacharjee, "Ku-band substrate integrated waveguide (SIW) slot array antenna for next generation networks," *Global Journal of Computer Science and Technology Network, Web & Security*, Vol. 13, No. 5, 11–16, 2013.

[27] Huang, T., G.-B. Liu, H.-F. Zhang, and L. Zeng, "A new adjustable frequency waveguide circularly polarized antenna based on the solid-state plasma," *Applied Physics A*, Vol. 125, 1–9, 2019.

[28] Mohammadi, S., J. Nourinia, C. Ghobadi, J. Pourahmadazar, and M. Shokri, "Compact broadband circularly polarized slot antenna using two linked elliptical slots for C-band applications," *IEEE Antennas and Wireless Propagation Letters*, Vol. 12, 1094–1097, 2013.

[29] Trinh-Van, S., Y. Yang, K.-Y. Lee, Y. S. Kim, and K. C. Hwang, "Bandwidth-enhanced circularly polarized crescent-shaped slot antenna via circular-patch loading," *Applied Sciences*, Vol. 9, No. 6, 1117, 2019.